Magnetocaloric effect in the low hysteresis Ni-Mn-In metamagnetic shape-memory Heusler alloy

Enric Stern-Taulats, Pedro O. Castillo-Villa, Lluís Mañosa, Carlos Frontera, Sabyasachi Pramanick, Subham Majumdar, and Antoni Planes

Citation: Journal of Applied Physics **115**, 173907 (2014);
View online: https://doi.org/10.1063/1.4874935
View Table of Contents: http://aip.scitation.org/toc/jap/115/17
Published by the American Institute of Physics

Magnetocaloric effect in the low hysteresis Ni-Mn-In metamagnetic shape-memory Heusler alloy

Enric Stern-Taulats,[1] Pedro O. Castillo-Villa,[1,2] Lluís Mañosa,[1] Carlos Frontera,[3] Sabyasachi Pramanick,[4] Subham Majumdar,[4] and Antoni Planes[1]
[1]*Departament d'Estructura i Constituents de la Matèria, Facultat de Física, Universitat de Barcelona, Diagonal 647, E-08028 Barcelona, Catalonia, Spain*
[2]*Instituto Potosino de Investigación Científica y Tecnológica, Camino a la Presa San José 2005, Col. Lomas 4a, CP.78216, San Luis Potosí, Mexico*
[3]*Institut de Ciència de Materials de Barcelona, Campus UAB, 08193 Bellaterra, Catalonia, Spain*
[4]*Department of Solid State Physics, Indian Association for the Cultivation of Science, Jadavpur, Kolkata 700 032, India*

(Received 3 February 2014; accepted 23 April 2014; published online 5 May 2014)

We have studied magnetocaloric properties of a Ni-Mn-In metamagnetic shape-memory alloy especially designed in order to display low thermal hysteresis. Magnetization and calorimetric measurements under a magnetic field have been used in order to determine isothermal magnetic field-induced entropy changes. Results obtained indirectly from magnetization data, quasi-directly from isofield calorimetric measurements, and directly from isothermal calorimetric runs are systematic and agree well with each other. We have analyzed the reproducibility of magnetocaloric properties with cycling from direct isothermal calorimetric measurements. Due to low thermal hysteresis, we have found that about 80% of the transition entropy change, $\Delta S_t \simeq 25$ J/kg K, can be reversibly induced under successive application and removal of a field of 6 T. © *2014 AIP Publishing LLC*.
[http://dx.doi.org/10.1063/1.4874935]

I. INTRODUCTION

Caloric effects rely on the thermal response of a given material to changes in an externally applied field.[1] When the field is modified isothermally the caloric effect is measured by an entropy change related to the heat exchanged with the surroundings. When the field is varied adiabatically the caloric effect is characterized by the induced change of temperature. Ferroic materials show large caloric effects in the vicinity of their transition to the ferroic phase.[2,3] Especially interesting are those materials where the ferroic transition is first order and can be field induced thus giving rise to large isothermal changes of entropy or large adiabatic changes of temperature, which, to a large extent, are provided by the transition latent heat. Ferromagnetic materials are prototypical examples of ferroic materials. Over the last two decades, a great deal of effort has been devoted to the search for new ferromagnetic materials displaying outstanding (or giant) magnetocaloric effects in the vicinity of room temperature due to their potential application in magnetic refrigeration devices.[4–6] More recently, this objective has been extended to the study of the electrocaloric effect[7,8] in ferroelectric materials and mechanocaloric effects[9,10] in ferroelastic/martensitic materials.

In a solid state refrigeration device, a giant caloric ferroic material is driven through successive cycles across the ferroic transition.[11,12] The corresponding adiabatic changes of temperature are obtained by adiabatic application and removal of a field. Optimal efficiency of this cycling process is favored by (i) a large transition entropy which measures the amount of heat that can be exchanged with the low and high temperature reservoirs and (ii) a marked sensitivity of the transition temperature to an applied field which is favored by both a fast and large change of the ferroic property at the ferroic transition. Notice that these two conditions require that the ferroic transition displays a significant first-order character which is often a consequence of a strong interplay of the primary ferroic property and structure. However, the possibility of inducing reproducible large adiabatic changes of temperature requires that the ferroic transition has sufficiently low thermal hysteresis[13–15] which, unfortunately, is intrinsically associated with first-order phase transitions and is enhanced when the transition involves a structural change. Therefore, the low hysteresis condition competes against the strong first-order character necessary for a giant caloric response. This is an essential point that needs to be taken into account in order to design materials displaying optimal caloric properties for refrigeration applications.

In this paper, we study the magnetocaloric effect in a Ni-Mn-In metamagnetic shape-memory alloy. Ni-Mn-In alloys belong to the family of NiMn-based Heusler alloys. The composition range of interest is, in general, a relatively narrow region shifted from the 2-1-1 Heusler stoichiometry.[16,17] In this range, on cooling, the material first becomes ferromagnetic and further transforms to a paramagnetic or antiferromagnetic martensite. Interestingly, large strains are available by magnetically inducing the reverse martensitic transition and therefore these systems display magnetic superelasticity. Associated with the complex magneto-structural interplay at the origin of this striking behavior,[18] these materials also show other interesting functional properties such as magneto-[19] and mechanocaloric effects,[10,20] magnetoresistence,[21] and exchange bias.[22] Among these properties, the magnetocaloric effect in Ni-Mn-In alloys has

been widely studied.[23–25] In the vicinity of the martensitic transition, these materials display the inverse magnetocaloric effect[26] which means that cooling occurs by adiabatic application of a magnetic field. When measured in terms of isothermal field-induced entropy changes, the thermal response of Heusler materials is perfectly comparable to that of the best magnetocaloric materials. However, the relatively large hysteresis associated with the martensitic transition strongly hampers the available cooling capacity in these alloys and therefore their performance in cooling devices. In the present paper, we have studied magnetocaloric properties of a Ni-Mn-In alloy, especially designed to display large enough entropy changes together with a low-temperature width of hysteresis and reasonably large temperature-shift of the whole hysteresis loop due to application of a magnetic field. The studied material has been grown with an appropriate composition for which optimal geometrical compatibility between low and high symmetry phases is expected. When this condition is satisfied, it has been shown[27,28] that the martensitic transition exhibits high reversibility and weak degradation during cycling.

The paper is organized as follows. In Sec. II, the experimental set-up, sample characteristics, and methods are described. The obtained magnetization and calorimetric results are presented and briefly discussed in Sec. III. In Sec. IV, we discuss magnetocaloric properties of the studied material. Finally, in Sec. V, the main conclusions are summarized.

II. EXPERIMENTAL DETAILS AND ALLOY DESIGN

A polycrystalline sample of nominal composition $Ni_{51}Mn_{33.4}In_{15.6}$ was prepared by arc-melting the pure metals under an argon atmosphere in a water-cooled Cu crucible. For homogeneity, the sample was remelted several times and, subsequently, the ingot was vacuum sealed in a quartz tube and annealed at 900 °C for 48 h followed by quenching in ice water. Specimens were cut with a diamond saw. A 105.7 mg sample with the shape of an eighth of an ellipsoid with 3.7, 2.7, 2 mm semi-axis was used for neutron diffraction and magnetic measurements, and a 372.5 mg sample with quarter ellipsoid shape with 5.4, 4.3, 3.6 mm semi-axis was used for calorimetric measurements. In all measurements, the magnetic field was applied along the direction of the long semi-axis.

The phase diagram of Ni-Mn-In alloys is shown in Fig. 1. Transition temperatures are plotted as a function of the valence electron concentration (e/a). Continuous lines are the fits to experimental data for quasi-stoichiometric $Ni_{50}Mn_{50-x}In_x$ alloys published in Ref. 19. Symbols correspond to published data for alloys of the Ni-rich, $Ni_{51}Mn_{49-x}In_x$, family. Open symbols are from Ref. 30 and solid symbols correspond to the alloy studied in the present paper. While the martensitic transition line for Ni-rich alloys is very close to quasi-stoichiometric alloys, the Curie line of the parent phase is located at slightly higher temperatures.

Neutron diffraction measurements were carried out by using the D1B high resolution neutron two-axis diffractometer at ILL under a flux at 2.52 Å. The polycrystalline sample was placed in an irradiated cylinder in permanent rotation

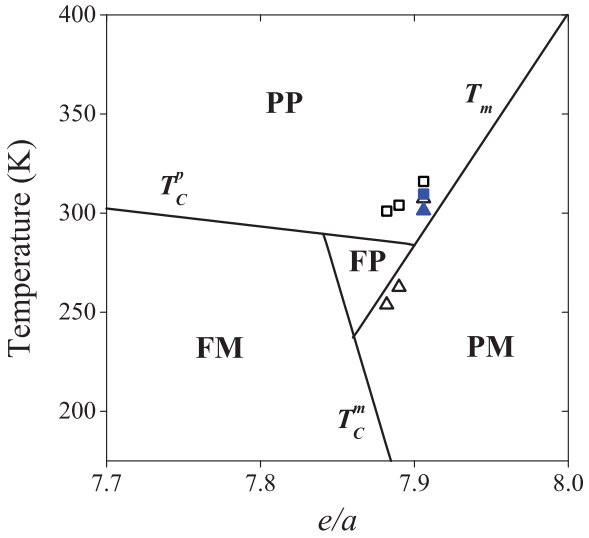

FIG. 1. Phase diagram of $Ni_{50}Mn_{50-x}In_x$ (continuous lines). Symbols correspond to $Ni_{51}Mn_{49-x}In_x$ alloys (squares: T_m, triangles: T_c^p). PP: paramagnetic parent phase, FP: ferromagnetic parent phase, PM: paramagnetic martensite, FM: ferromagnetic martensite. T_m: martensitic transition, T_c^p: Curie temperature of the parent phase, T_c^m: Curie temperature of the martensitic phase.

with the use of a rotator device in order to prevent prevalent contributions to the diffraction spectra. 1 h exposure time measurements were performed under isothermal conditions.

Analysis of neutron diffraction patterns collected at 325 and 280 K (shown in Fig. 2) evidences the existence of a structural phase transition. The pattern collected at 325 K can be indexed with a cubic cell (space group $Fm3m$ no. 225) with $a = 6.008(2)$ Å. This structure corresponds to the parent phase. At 280 K, the neutron diffraction pattern can be indexed with a monoclinic cell (average structure) with $a = 4.394(1)$ Å, $b = 5.640(2)$ Å, $c = 4.340(1)$ Å, and $\beta = 86.88(3)°$. This is the martensitic phase.

Hysteresis is to a large extent determined by a geometric compatibility condition between parent and martensitic phases in martensitic materials. When this condition is satisfied the martensitic transition occurs with very low hysteresis.[28] Theoretically, it has been shown that this condition can be quantified through the cofactor conditions which can be determined once lattice parameters of the high and low

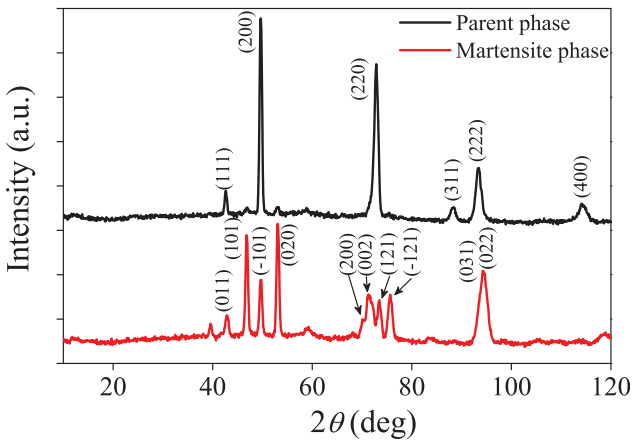

FIG. 2. Neutron diffraction patterns of the sample in the parent (325 K) and martensitic (280 K) phases.

symmetry phases are known.[27] From the obtained cell parameters above and below the martensitic transition, we have determined these cofactor conditions by using the procedures explained in Ref. 31. From the analysis, we have obtained quite a good compatibility of parent/twinned martensite interfaces. Specifically, we have found that the middle eigenvalue of the stretch tensor **U**, $\lambda_2 = 0.9981(15)$, and the norms X_{I} and X_{II} for type I and II twins are 0.9985 and 1.0084 (for $\hat{e} = [110]/[1\bar{1}0]$), respectively. Ideal compatibility requires that $\lambda_2 = 1$ and X_{I} or $X_{\mathrm{II}} = 1$. Our values deviate from ideal compatibility by less than 0.2% which anticipates that thermal hysteresis should be very small in the studied material.

Magnetization was measured by using a superconducting quantum interferometer device (SQUID, Quantum Design). Measurements were done under applied fields ranging between 0.005 and 5 T in cooling-heating cycles between 280 and 320 K at a rate of 0.4 K/min.

Calorimetric measurements were performed by using a purpose-built calorimeter capable of operating under external magnetic fields described in Ref. 33. The set-up allows isofield measurements to be performed by scanning the temperature and isothermal measurements to be done by scanning the magnetic field.

III. RESULTS: MAGNETOMETRY AND CALORIMETRY

A. Magnetometry

Fig. 3 shows magnetization versus temperature measurements $M_{p(m)}(T, H)$ during heating and cooling runs across the martensitic and ferromagnetic transitions for selected values of the applied magnetic field (isofield measurements). Hereafter, the sub-indices p and m will indicate measurements performed during reverse and forward martensitic transitions. Results show that the paramagnetic martensite phase structurally transforms on heating to a ferromagnetic parent phase. The Curie point of the parent phase is located from measurements at low applied magnetic field at $T_c \simeq 309.5$ K as indicated in the inset of Fig. 3. The existence of

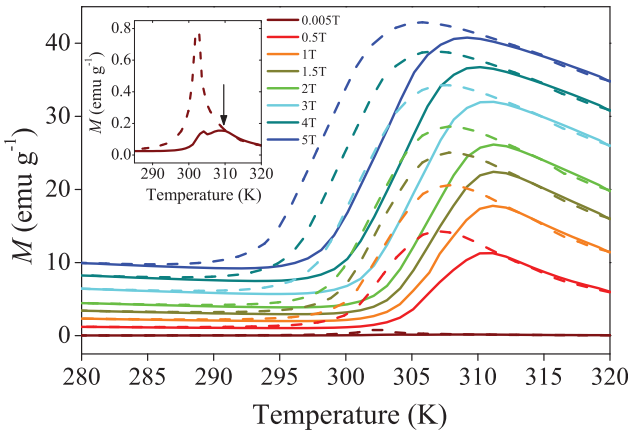

FIG. 3. Magnetization versus temperature curves at selected applied magnetic fields [indicated in the legend] obtained upon heating (continuous lines) and cooling (dashed lines). The inset shows a low-field measurement from which the Curie temperature has been identified. T_c is indicated with the arrow.

a martensitic transition is revealed by the sharp change of magnetization as temperature is increased or decreased. This behavior is in agreement with the significant first-order character of the martensitic transition. The corresponding change of magnetization, $\Delta M_{tp(m)}$, can be estimated for each applied magnetic field as the magnetization difference at the transition temperature between extrapolations of the linear behavior of $M_{p(m)}$ vs. T curves well above and well below the transition. Transition temperatures have been identified with inflection points in the magnetization curves. We will denote T_p and T_m as the corresponding transition temperatures of the reverse (heating) and forward (cooling) transitions. Note that the difference $T_p - T_m$ ($\sim$4 K) provides a measure of the thermal hysteresis of the transition. It is found that to within error hysteresis remains independent of the applied magnetic field. Note that the value of the hysteresis is quite small and is comparable to that of low-hysteresis martensitic materials.[31]

$\Delta M_{tp(m)}$ and transition temperatures are plotted as a function of the applied magnetic field for heating and cooling runs in Figs. 4(a) and 4(b), respectively. It is interesting to note that as magnetic fields are increased, the martensitic transition temperatures shift towards lower temperatures. From the rates dT_p/dH and dT_m/dH corresponding to the reverse and forward transitions, respectively, and the changes of magnetization at the transition, transition entropy changes $\Delta S_{tp(m)}$ can be estimated from the Clausius-Clapeyron equation. That is

$$\Delta S_{t_{p(m)}} = -\mu_0 \Delta M_{t_{p(m)}}(T, H)\left(\frac{dT_{p(m)}}{dH}\right)^{-1}. \quad (1)$$

The obtained results are shown in Figure 4(c). It is obtained that the transition entropy change (absolute value) slightly decreases with increasing the applied magnetic field.

B. Calorimetry

1. Isofield calorimetry

Thermal curves obtained from temperature scans performed at a rate 0.4 K/min and selected applied magnetic fields (isofield measurements) are shown in Figs. 5(a) and 5(b). Positive peaks (endothermal) correspond to reverse martensitic transitions, while negative peaks (exothermal) correspond to forward transitions. The figures clearly show that as the applied field is increased the peaks shift to lower temperatures. No anomaly associated with the occurrence of the paramagnetic-ferromagnetic transition at T_c is detected in the thermal curves due to the overlap of both first- and second-order structural and magnetic transitions and the prevalence of the peak associated with the structural transition which involves a large latent heat. The maxima of the thermal curves must be identified with the temperatures T_p and T_m. These temperatures are plotted in Fig. 4(b). Note that the obtained values slightly deviate from those determined from the inflection point of magnetization curves. This is likely to be due to the fact that calorimetric and magnetization measurements have been performed on different specimens. Nevertheless, hysteresis is very similar in both

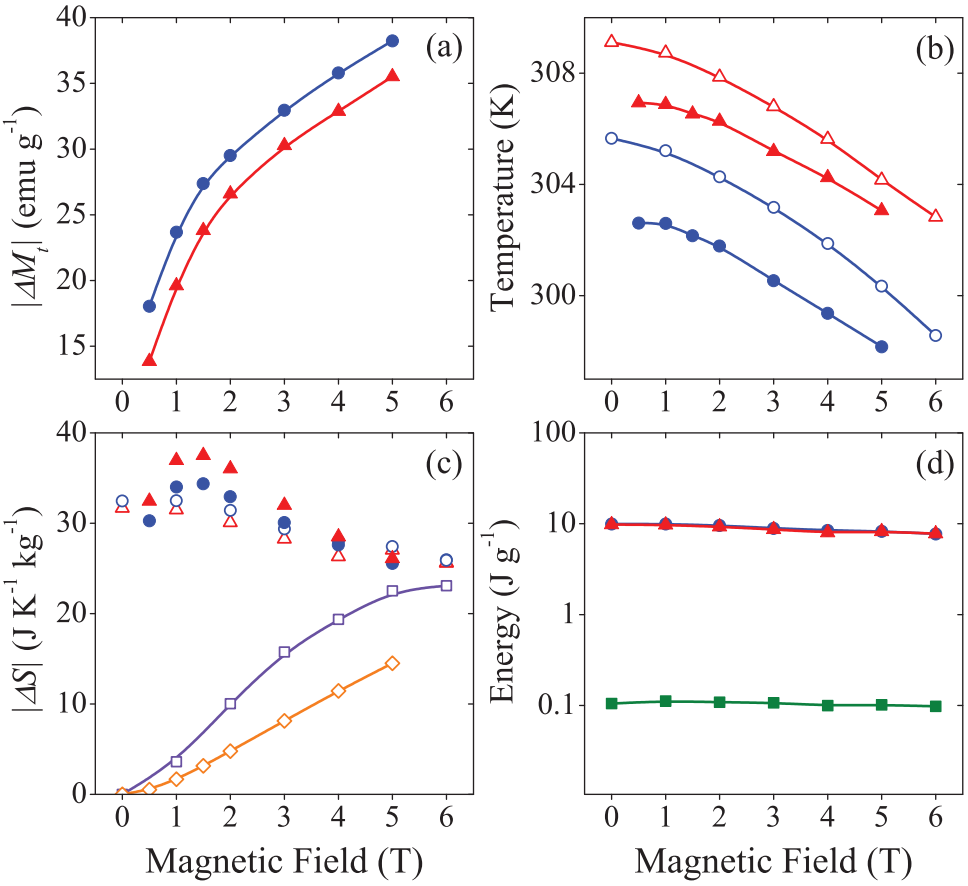

FIG. 4. Magnetization changes $\Delta M_{tp(m)}$ from the martensitic transition as a function of the applied magnetic field, $\mu_0 H$, are plotted in (a). Panel (b) shows transition temperatures as a function of the applied magnetic field from both magnetometry (solid symbols) and calorimetry (open symbols) measurements. Red triangles refer to heating runs and blue circles refer to cooling. With the same symbols, panel (c) shows the transition entropy changes obtained either from the isofield calorimetric curves or from the Clausius-Clapeyron equation. For the sake of comparison, violet squares indicate the quasi-direct maximum field-induced entropy change obtained at each applied field change $\mu_0 \Delta H$. Orange squares correspond to the maximum value of the field-induced entropy change obtained from magnetization curves. Panel (d) shows the latent heat (enthalpy changes L of the martensitic transition) computed from the isofield calorimetric curves (red and blue solid symbols) and the dissipated energy E_{diss} (green solid squares) on a logarithmic scale.

cases. Partial integration of the thermal curves given in Figs. 5(a) and 5(b) from a temperature T_0^m below the end temperature of the forward transition to a temperature T enables entropy curves at each applied magnetic field to be obtained. These curves describe the variation of the entropy with temperature for reverse and forward transformation processes from a reference entropy S_0^m associated with the martensitic phase. That is

$$S_{p(m)}(T,H) = S_0^m + \int_{T_0^m}^{T} \frac{1}{T} \frac{\dot{q}_{p(m)}(T,H)}{\dot{T}} dT, \qquad (2)$$

where $\dot{q}_{p(m)}$ is the thermal signal provided by the calorimeter and $\dot{T}$ is the local temperature rate. It is worth noting that in the preceding expression, integration is performed with respect to a suitable base-line and thus only the contribution to the entropy from the transition is taken into account. Note that total integration up to a temperature above the end temperature of the reverse transition or the start temperature of the forward transition provide the martensitic transition entropy change $\Delta S_{t_{p(m)}} = S_{p(m)}(T,H) - S_0^m$ for the reverse and forward transitions, respectively. The obtained values for heating and cooling runs are plotted in Fig. 4(c) and can be compared to the estimates derived from the Clausius-Clapeyron equation. Reasonably good agreement is obtained for all values to within errors.

At each temperature in the interval between the reverse or forward transformation regions, the fraction of parent phase $x_{p(m)}(T,H)$ can be computed from normalization of entropy curves with respect to transition entropy. That is

$$x_{p(m)}(T,H) = \frac{S_{p(m)}(T,H) - S_0^m}{\Delta S_{t_{p(m)}}}. \qquad (3)$$

The dissipated energy, E_{diss}, associated with transformation hysteresis can be estimated as the area of the hysteresis cycle in entropy-temperature space. Therefore, it can be expressed as

$$E_{diss} = \Delta S_t \left[\int_{T_0^m}^{T_0^p} x_p dT + \int_{T_0^p}^{T_0^m} x_m dT \right], \qquad (4)$$

where T_0^p is a temperature above the end temperature of the reverse transition, and ΔS_t is the transition entropy change computed as an average value between heating and cooling runs, $\Delta S_t = (\Delta S_p + \Delta S_m)/2$. It is interesting to compare this

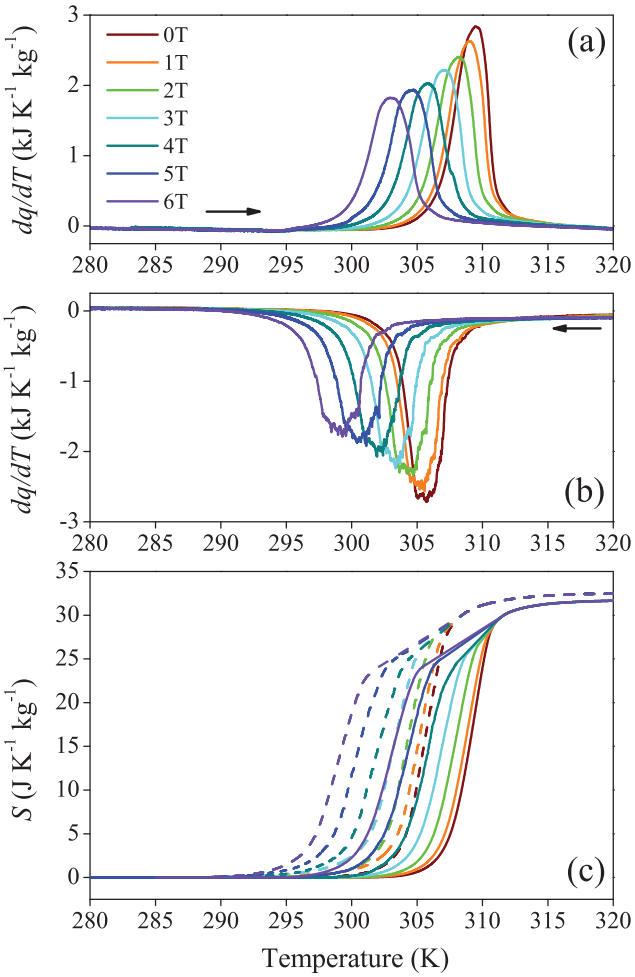

FIG. 5. Isofield calorimetric curves at selected values of the applied magnetic field. (a) Heating runs, (b) cooling runs, and (c) entropy curves for cooling (dashed lines) and heating (continuous lines) runs.

dissipated energy with the transition latent heat that can be estimated as $L \simeq T_t \Delta S_t$, where $T_t = (T_p + T_m)/2$. The latent heat and the dissipated energy are plotted (on a logarithmic scale) as a function of the applied magnetic field in Fig. 4(d). Both energies remain independent of the applied field to a good approximation. Results show that the dissipated energy is very small, two orders of magnitude lower than the latent heat ($E_{diss}/L \simeq (T_p - T_m)/T_t \sim 10^{-2}$).

2. Isothermal calorimetry

Taking into account the fact that in the studied materials the transition shifts to a lower temperature under an applied magnetic field, isothermal calorimetric measurements have been performed according to the following protocol. In the case of the forward transition (exothermal), the sample is first magnetized under a high applied field ($\mu_0 H = 6\,\mathrm{T}$) at low temperature (martensitic phase) and then heated up to the full parent phase. It is then cooled down to the measurement temperature. Keeping this temperature constant, the removal of the magnetic field drives the structural transition to a state with a higher fraction of martensite, which gives rise to a negative (exothermal) peak in the calorimetric signal (i.e., $\Delta S < 0$). On the other hand, for the reverse transition the sample is first cooled down at zero field to a full martensitic state, and it is then heated up to the measurement temperature. When the magnetic field is isothermally increased, the reverse transition occurs giving rise to a positive (endothermal) peak. For these measurements, the magnetic field sweeping rate was ∓ 0.44 T/min for forward and reverse transitions, respectively.

Examples of calorimetric curves (represented as heat released/absorbed per unit of magnetic field change vs. magnetic field) corresponding to the first isothermal magnetic field scans obtained at selected temperatures are shown in Figure 6(a). Panels (b) and (c) show the results corresponding to magnetic field cycling at selected temperatures. Calorimetric curves are represented here as released/absorbed heat flow versus time. Examples shown in panel (b) start in

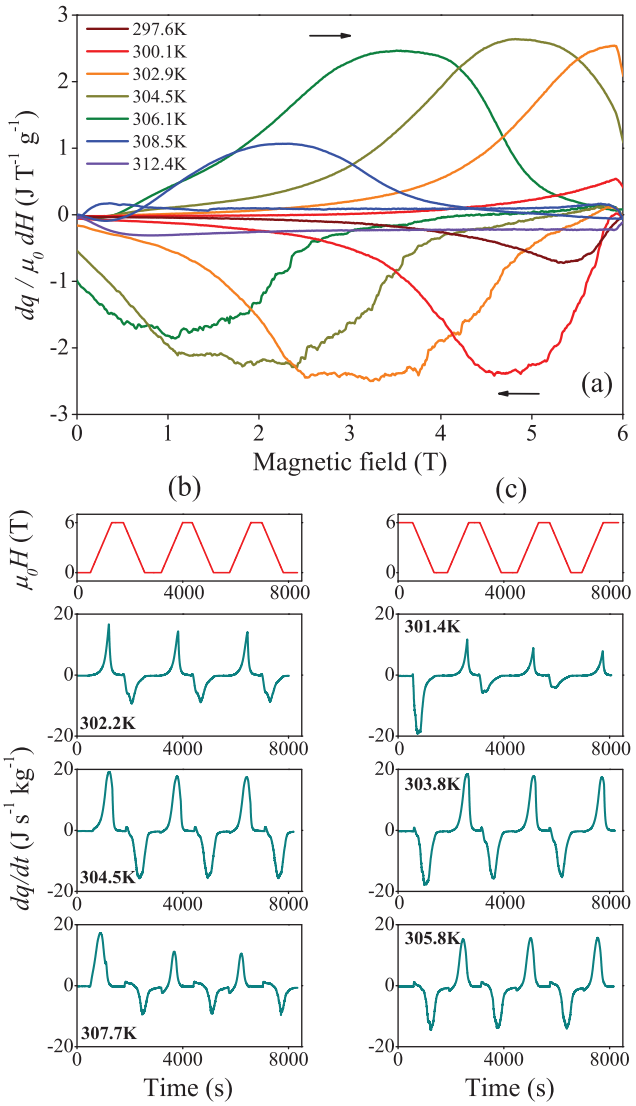

FIG. 6. (a) Calorimetric curves obtained upon first application of the magnetic field (negative peaks) and first removal of magnetic field (positive peaks) at several representative temperatures. Panels (b) and (c) show calorimetric curves obtained upon consecutive magnetic field scans at selected temperatures. Calorimetric curves in panel (b) correspond to cycles that begin with an application of the magnetic field ($0\,T \rightarrow 6\,T$), whereas calorimetric curves shown in panel (c) are those where the magnetic field is first removed ($6\,T \rightarrow 0\,T$). The upper figures in panels (b) and (c) show the time variation of the applied magnetic field.

the martensitic phase by application of the field [as indicated in the upper plot of Fig. 6(b)], while in (c) the system is initially in the parent phase and the field is first removed [as seen in the upper plot of Fig. 6(c)]. It is worth pointing out that measurement protocol prevents the influence of hysteresis in the first application/removal of the magnetic field. In subsequent cycles, only the reversible contribution is detected.

IV. MAGNETOCALORIC EFFECT

The magnetocaloric effect in the vicinity of the magnetostructural martensitic transition can be quantified from the entropy change induced from the isothermal application or removal of a given magnetic field. This entropy change can be obtained from both magnetization (indirect method) and calorimetric measurements (quasi-direct and direct methods). From magnetization curves, it can be determined as

$$\Delta S_{p(m)}[T, 0(H) \rightarrow H(0)] = \mu_0 \int_{0(H)}^{H(0)} \left(\frac{\partial M_{p(m)}}{\partial T}\right)_H dH, \quad (5)$$

which is obtained from integration of the Maxwell relation $(\partial S/\partial H)_T = \mu_0(\partial M/\partial T)_H$. Results giving ΔS computed from this indirect method as a function of T for heating (p) and cooling (m) runs at given values of the magnetic field are shown in Fig. 7, for fields (applied/removed) up to 5 T. Clearly, the magnetocaloric effect increases in magnitude by increasing the applied magnetic field. For a field of 5 T, a maximum value of about 15 J/K kg is obtained. Note that the magnetocaloric effect is inverse, which is consistent with the fact that transition temperatures shift to lower values under an applied magnetic field.

Isothermal field-induced entropy changes can also be obtained from isofield calorimetric data. From this quasi-direct method, entropy changes are computed from substraction, at each temperature, of the calorimetric entropy curves shown in Fig. 5(c). As previously indicated, integration of calorimetric curves is performed with respect to a base line, which excludes any background entropy contribution related to a difference of heat capacity, ΔC, between both martensitic and parent phases. This effect can be taken into account from the temperature dependence of the entropy change since

$$\frac{\Delta C}{T} = \frac{\partial \Delta S_t}{\partial T}. \quad (6)$$

This slope is plotted in Fig. 5(c) and is taken into account when substracting the calorimetric entropy curves in order to obtain field-induced entropy changes. The results obtained from this method are depicted as solid lines in Fig. 8 for fields (applied/removed) up to 6 T. The magnetocaloric effect increases in magnitude by increasing the applied magnetic field and tends to reach a saturation value for fields above 5 T. The maximum value of the field-induced entropy change has been plotted in Fig. 4(c), which shows that the saturation value coincides, as expected, with the total transition entropy change. It is worth noting that at each field, the field-induced entropy change obtained from calorimetric measurements is slightly larger than the entropy change obtained from magnetization measurements [see Fig. 4(c)]. While the difference could be ascribed to the fact that different specimens are used in calorimetric and magnetization

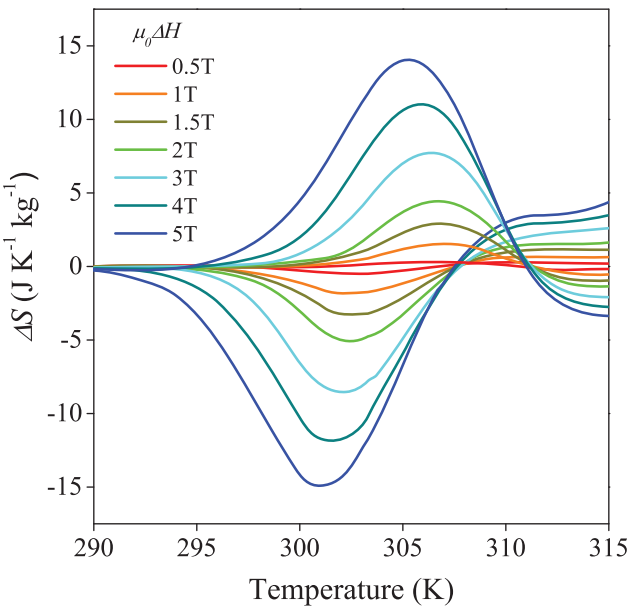

FIG. 7. Field-induced entropy changes at selected values of the applied/removed magnetic field (indicated in the figure) from magnetization measurements.

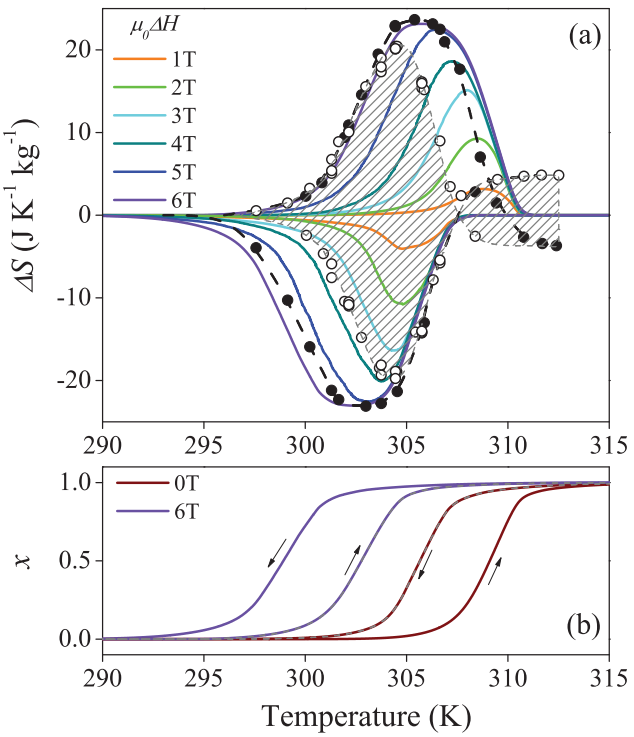

FIG. 8. (a) Magnetic entropy change $\Delta S(\mu_0\Delta H)$ obtained from quasi-direct computation are plotted with colored lines. Each color refers to the field change $\mu_0\Delta H$. Black solid circles refer to entropy changes from the first magnetic field ramps from isothermal calorimetry. Open circles refer to entropy changes from subsequent field cycling. Dashed lines are a guide for the eye. The reversibility region is dashed with grey lines. (b) Transformed fraction curves upon heating and cooling at zero field and high field ($\mu_0 H = 6\,T$). The reversible region that separates the loops at zero and 6 T is dashed with grey lines.

measurements, it must also be considered that the quasi-direct calorimetric method only takes into account the contribution to the entropy change arising from the transition itself. Since the contribution from outside the transition has the opposite sign ($\partial M/\partial T < 0$) to the contribution from the transition ($\partial M/\partial T > 0$), indirect estimations based on magnetization measurements should (in absolute values) be lower than the quasi-direct estimations. In any case, note that only the high temperature contribution from outside the transition is relevant since in the martensitic phase $\partial M/\partial T \simeq 0$ to a good approximation.

Isothermal calorimetry provides a method to directly determine field-induced entropy changes. From thermal curves obtained at T by sweeping the magnetic field, entropy changes can be computed as

$$\Delta S_{p(m)}[T, 0(H) \rightarrow H(0)] = \frac{1}{T}\int_{0(H)}^{H(0)} \frac{\dot{q}_{p(m)}(T,H)}{\dot{H}} dH, \qquad (7)$$

where $\dot{H}$ is the rate at which the field has been swept. The integration baseline must be chosen in such a way that in addition to the contribution from the transition, the effect of a difference of heat capacities between both parent and martensitic phase is taken into account. Therefore, this method should provide estimations comparable to those obtained from the calorimetric quasi-direct method. Results obtained in the first cycle by application and removal of a magnetic field of 6 T are shown as solid symbols in Fig. 8(a). The agreement with quasi-direct measurements is very good. Only the right-hand side of the curves corresponding to temperatures close to the ferromagnetic-paramagnetic transition shows some discrepancies. These differences arise from the conventional magnetocaloric effect associated with this ferromagnetic-paramagnetic transition which is taken into account in direct calorimetric measurements, but not in quasi-direct measurements. The same conventional contribution at high temperatures is in fact observed in magnetocaloric curves obtained from magnetization measurements (see Fig. 7).

Results obtained upon further magnetic field cycling (up to 6 T) are shown in Fig. 8(a) as open symbols. Compared with the first cycle, a lower field-induced entropy change is obtained. Interestingly, these values are reproducible from cycle to cycle and thus define a reversible region which is shown as a shadowed area in Fig. 8. For an applied field $\mu_0\Delta H = 6$ T, the maximum value of the reversible entropy change is 20 J K^{-1} kg^{-1} which represents more than 80% of the total magnetocaloric entropy change obtained at the first magnetic field ramp.

The reversibility of the magnetocaloric effect depends crucially on competition between the width of thermal hysteresis and the sensitivity of transition temperatures upon an applied magnetic field. A narrow hysteresis and a large shift of transition temperatures with the applied field favor reversibility. For a given hysteresis, substantial reversibility occurs when the shift of forward and reverse transition temperatures is larger than hysteresis. That is, the magnetic field-induced shift of the whole hysteresis loop must be larger than thermal hysteresis. This is illustrated in Fig. 8(b) which shows hysteresis loops (represented as the fraction of parent phase vs. temperature) for applied magnetic field of zero and 6 T. Comparing panels (a) and (b), it is clear that the reversible region of the magnetocaloric effect corresponds to the temperature interval that separates these two loops [shadowed area in panel (b)]. In other words, reversible values for the magnetocaloric effect are found within a temperature interval bounded by the start of the forward martensitic transition at zero field and the start of the reverse transition under an applied field. Actually, in this temperature region, the magnetic field carries the state of the material through a minor hysteresis loop,[29] and the reversibility in the magnetocaloric effect is directly related to the reversibility in the fraction of material that undergoes the forward and reverse transition in the cycle. Of course, when the size of the shift in martensitic transition temperatures due to the magnetic field is large enough, the minor loops approach the full transformation loop and a maximum reversible magnetocaloric effect is obtained.

Magnetocaloric properties of Ni-Mn-In alloys with composition similar to the material studied in the present paper have been reported in Refs. 30 and 34. In the first of these papers, the authors studied the influence of composition on magnetocaloric properties in $Ni_{51}Mn_{49-x}In_x$ alloys. The martensitic transition was found to show minimum hysteresis close to $x = 15.6$ which corresponds to the composition studied in the present paper. From our results, this minimum value is explained due to the optimal compatibility between parent and martensitic structures. Interestingly, a maximum isothermal magnetic field-induced entropy change associated with the martensitic transition was also observed close to the same composition, $x = 15.6$. Actually, this is the result that we would expect taking into account the fact that for $x = 15.6$ martensitic and magnetic transitions are almost coincident, and the transition entropy change in Ni-Mn-In alloys is known to decrease when increasing the separation between magnetic and martensitic transitions.[35,36] This behavior is a consequence of the competition between structural and magnetic contributions to the entropy change which have opposite signs.[37]

In Ref. 34, adiabatic field-induced temperature changes for an alloy with $x = 15.6$ have been reported. For the studied alloy, the hysteresis was much larger than in our case. During heating, temperature changes of 1 K/T were obtained while changes of 0.5 K/T were found during cooling. These values are slightly lower than our estimations of the shift of martensitic transition under an applied field obtained in the present paper.

V. SUMMARY AND CONCLUSIONS

We have studied MCE at room temperature in a low hysteresis $Ni_{51}Mn_{33.4}In_{15.6}$ metamagnetic shape-memory alloy by means of magnetometry and differential scanning calorimetry measurements. Good consistence has been found between both experimental methods and the derivation of the MCE features using direct, quasi-direct, and indirect methods.

The alloy composition has been designed so that high and low symmetry phases satisfy optimal geometric

compatibility conditions. Compatibility has been quantified by cofactor conditions. From lattice parameters determined from neutron scattering experiments, we have shown that these conditions deviate less than 0.2% from the expected ideal situation in our alloy. This ensures that the martensitic transition in our alloy occurs with a high degree of reversibility measured by a thermal hysteresis as low as 4 K.

Despite the fact that transition temperatures show only moderate sensitivity to an applied magnetic field, the small hysteresis of the transformation enables large reversible entropy changes up to $20\,J\,K^{-1}\,kg^{-1}$ with successive application and removal of a magnetic field of 6 T. Overall, for a given magnetic field, in the vicinity of a magnetostructural first-order transition, the magnetocaloric reversible region extends from the start temperature of the forward transition at zero field to the start temperature of the reverse transition under applied field. The rule indeed applies to direct, quasi-direct, and indirect kind of measurement used to quantify the magnetocaloric effect.

It is worth mentioning that a similar strategy to the one followed in the present paper was already proposed by Srivastava *et al.*[32] in order to design Heusler alloys with low hysteresis. A $Ni_{45}Co_5Mn_{20}Sn_{10}$ alloy with λ_2 only slightly greater than 1 was shown to display a relatively low thermal hysteresis of about 6 K. Similar to our case, the compatibility condition was found to occur in an alloy with martensitic and Curie temperatures very close each other. Whether or not this is a general condition related to the interplay between magnetism and structure in this class of Heusler alloy or simply a mere coincidence is a point that warrants further investigation in the future.

ACKNOWLEDGMENTS

This work was supported by CICyT (Spain), Project No. MAT2013-40590-P, Joint Indo-Spanish project, DGICyT (Spain), Project No. PRI-PIBIN-2011-0780, and DST(India) Project No. DST/INT/P-39/11. E.S.-T. acknowledges support from AGAUR (Catalonia). P.C.-V. acknowledges support from CONACYT (México) under Scholarship No. 186474.

[1]X. Moya, S. Kar-Narayan, and N. D. Mathur, Nature Mater. **13**, 439 (2014).
[2]L. Mañosa, A. Planes, and M. Acet, J. Mater. Chem. A **1**, 4925 (2013).
[3]S. Fähler, U. K. Rößler, O. Kastner, J. Eckert, G. Eggeler, H. Emmerich, P. Entel, S. Müller, E. Quandt, and K. Albe, Adv. Eng. Mater. **14**, 10 (2012).
[4]A. M. Tishin, *Handbook of Magnetic Materials*, edited by K. H. J. Buschow (Elsevier Science, Amsterdam, 1999),Vol. 12, pp. 395–524.
[5]K. A. Gschneidner, V. K. Pecharsky, and A. O. Tsokol, Rep. Prog. Phys. **68**, 1479 (2005).
[6]A. Smith, C. R. H. Bahl, R. Bjørk, K. Engelbrecht, K. K. Nielsen, and N. Pryds, Adv. Energy Mater. **2**, 1288 (2012).
[7]A. S. Mishenko, Q. Zhang, J. F. Scott, R. W. Whatmore, and N. D. Mathur, Science **311**, 1270 (2006).
[8]X. Moya, E. Stern-Taulats, S. Crossley, D. González-Alonso, S. Kar-Narayan, A. Planes, L. Mañosa, and N. D. Mathur, Adv. Mater. **25**, 1360 (2013).
[9]E. Bonnot, R. Romero, E. Vives, L. Mañosa, and A. Planes, Phys. Rev. Lett. **100**, 125901 (2008).
[10]L. Mañosa, D. González-Alonso, A. Planes, E. Bonnot, M. Barrio, J. L. Tamarit, S. Aksoy, and M. Acet, Nature Mater. **9**, 478 (2010).
[11]A. M. Tishin and Y. I. Spichkin, *The Magnetocaloric Effect and its Applications* (Institute of Physics Publishing, Bristol, 2003).
[12]E. Brück, *Handbook of Magnetic Materials*, edited by K. H. J. Buschow (Elsevier Science, Amsterdam, 2008),Vol. 17, pp. 235–291.
[13]T. Krenke, S. Aksoy, E. Duman, M. Acet, X. Moya, L. Mañosa, and A. Planes, J. Appl. Phys. **108**, 043914 (2010).
[14]V. V. Khovaylo, K. P. Skokov, O. Gutfleisch, H. Miki, R. Kainuma, and T. Kanomata, Appl. Phys. Lett. **97**, 052503 (2010).
[15]V. Basso, C. P. Sasso, K. P. Skokov, O. Gutfleisch, and V. V. Khovaylo, Phys. Rev. B **85**, 014430 (2012).
[16]Y. Sutou, Y. Imano, N. Koeda, T. Omori, R. Kainuma, K. Ishida, and K. Oikawa, Appl. Phys. Lett. **85**, 4358 (2004).
[17]T. Krenke, M. Acet, E. F. Wassermann, X. Moya, L. Mañosa, and A. Planes, Phys. Rev. B **73**, 174413 (2006).
[18]M. Acet, L. Mañosa, and A. Planes, *Handbook of Magnetic Materials*, edited by K. H. J. Buschow (Elsevier Science, Amsterdam, 2011),Vol. 19, pp. 231–289.
[19]A. Planes, L. Mañosa, and M. Acet, J. Phys. Condens. Matter **21**, 233201 (2009).
[20]P. O. Castillo-Villa, D. E. Soto-Parra, J. A. Matutes-Aquino, R. A. Ochoa-Gamboa, A. Planes, L. Mañosa, D. González-Alonso, M. Stipcich, and R. Romero, Phys. Rev. B **83**, 174109 (2011).
[21]V. K. Sharma, M. K. Chattopadhyay, K. H. B. Shaeb, A. Chouhan, and S. B. Roy, Appl. Phys. Lett. **89**, 222509 (2006).
[22]S. Giri, M. Patra, and S. Majumdar, J. Phys. Condens. Matter **23**, 073201 (2011).
[23]Z. D. Han, D. H. Wang, C. L. Zhang, S. L. Tang, B. X. Gu, and Y. W. Du, Appl. Phys. Lett. **89**, 182507 (2006).
[24]T. Krenke, M. Acet, E. F. Wassermann, X. Moya, L. Mañosa, A. Planes, E. Suard, and B. Ouladdiaf, Phys. Rev. B **75**, 104414 (2007).
[25]P. A. Bhobe, K. R. Priolkar, and A. K. Nigam, Appl. Phys. Lett. **91**, 242503 (2007).
[26]T. Krenke, E. Duman, M. Acet, E. F. Wassermann, X. Moya, L. Mañosa, and A. Planes, Nature Mater. **4**, 450 (2005).
[27]R. D. James and Z. Zhang, in *Magnetism and Structure in Functional Materials*, edited by A. Planes, L. Mañosa, and A. Saxena (Springer-Verlag, 2005), pp. 159–175.
[28]Z. Zhang, R. D. James, and S. Müller, Acta Mater. **57**, 4332 (2009).
[29]I. Titov, M. Acet, M. Farle, D. González-Alonso, L. Mañosa, A. Planes, and T. Krenke, J. Appl. Phys. **112**, 073914 (2012).
[30]F. X. Hu, J. Wang, J. Shen, B. Gao, J. R. Sun, and B. G. Shen, J. Appl. Phys. **105**, 07A940 (2009).
[31]Y. Song, V. Dabade, T. W. Shield, and R. D. James, Nature **502**, 85 (2013).
[32]V. Srivastava, X. Chen, and R. D. James, Appl. Phys. Lett. **97**, 014101 (2010).
[33]B. Emre, S. Yüce, E. Stern-Taulats, A. Planes, S. Fabbrici, F. Albertini, and L. Mañosa, J. Appl. Phys. **113**, 213905 (2013).
[34]H. M. Seyoum, M. Ghahremani, H. ElBideihy, L. H. Bennett, E. Della Torre, F. Johnson, and M. Zuo, IEEE Magn. Lett. **4**, 6000204 (2013).
[35]W. Ito, Y. Imano, R. Kainuma, Y. Sutou, K. Oikawa, and K. Ishida. Metall. Mater. Trans. A **38**, 759 (2007).
[36]S. Kustov, M. L. Corró, J. Pons, and E. Cesari, Appl. Phys. Lett. **94**, 191901 (2009).
[37]A. Planes, L. Mañosa, and M. Acet, Mater. Sci. Forum **738–739**, 391 (2013).